BEST AVAILABLE IMAGES

Defective images within this document are accurate representations of the original documents submitted by the applicant.

Defects in the images may include (but are not limited to):

- BLACK BORDERS
- TEXT CUT OFF AT TOP, BOTTOM OR SIDES
- FADED TEXT
- ILLEGIBLE TEXT
- SKEWED/SLANTED IMAGES
- COLORED PHOTOS
- BLACK OR VERY BLACK AND WHITE DARK PHOTOS
- GRAY SCALE DOCUMENTS

IMAGES ARE BEST AVAILABLE COPY.

As rescanning documents *will not* correct images, please do not report the images to the Image Problem Mailbox.

Pergamon

Acta mater. Vol. 46, No. 10, pp. 3619–3635, 1998

Printed in Great Britain
PII: S1359-6454(98)00031-7
1359-6454/98 $19.00 + 0.00

HEAT TRANSFER IN OPEN-CELL METAL FOAMS

T. J. LU[1], H. A. STONE[2] and M. F. ASHBY[1]

[1]Department of Engineering, University of Cambridge, Cambridge CB2 1PZ, U.K. and [2]Division of Engineering and Applied Sciences, Harvard University, Cambridge, MA 02138, U.S.A.

(Received 29 October 1997; accepted 28 December 1997)

Abstract—The paper explores the use of open-celled metal foams as compact heat exchangers, exploiting convective cooling. An analytical model is developed for *model* foams with simple cubic unit cells consisting of heated slender cylinders, based on existing heat transfer data on convective crossflow through cylinder banks. A foam-filled channel having constant wall temperatures is analyzed to obtain the temperature distribution inside the channel as a function of foam density, cell size and other pertinent heat transfer parameters. Two characteristic length scales of importance to the problem are discussed: the minimum channel length required for heating the fluid to its goal temperature and the thermal entry length beyond which the transfer of heat between fluid and channel wall assumes a constant coefficient. The overall heat transfer coefficient of the heat exchanging system is calculated, and the pressure drop experienced by the fluid flow obtained. These results are used to analyze and guide the design of optimum foam structures that would maximize heat transfer per unit pumping power. Two examples are given to demonstrate the applicability of the analytical model: heat sinks for high power electronic devices and multi-layered heat exchangers for aeronautical applications. The present model perhaps oversimplifies the calculation of transport in a metal foam consisting of non-circular, possibly sharp-edged ligaments, and so likely leads to overestimates. Nevertheless the trends of heat transfer predicted by the model (for dependence on foam relative density, duct geometries, fluid velocity, etc.) are expected to be valid for a wide range of open-cell foams and are in reasonable agreement with available experimental data on aluminum foams (Bastawros and Evans, *Proc. Symp. Application of Heat Transfer in Microelectronics Packaging*. IMECE, Dallas, TX, 1997). © *1998 Acta Metallurgica Inc.*

1. INTRODUCTION

Non-metallic cellular foams, especially those based on polymers and ceramics, are widely used in thermal-insulation applications where their low thermal conductivity is exploited. The long list of application areas includes packaging of food, disposable hot-drink cups [1], chemical catalytic reactors, packed cryogenic microsphere insulations [2–4], solar-energy utilization, transpiration cooling [5], and cavity–wall insulation (dwellings, aircraft, submarine cabins, and so on). Heat is transported through these foams via three competing mechanisms: solid conduction, thermal radiation and fluid conduction. (Natural) convection within the cell is negligible, if the cell has a size less than 10 mm [1] and, on the scale of a cell, the typical temperature differences between the fluid and the solid cell edges are small. At room temperature, the thermal conductivities of most non-metal foams are well below 1 W/(m K), with those of polystyrene, polyurethane and phenolic foams having low relative densities (~0.02) roughly equal that of air, ~0.025 W/(m K).

Metal foams, on the other hand, are more likely to find applications in ultralight structures where stiffness, strength and toughness are emphasized. The effective thermal conductivities of open-celled metal foams, about one to two thirds of the product of their relative density and the thermal conductivity of the solid of which they are made, are at least one order of magnitude larger than those of their non-metallic counterparts [1], hence are generally unsuited for thermal-insulation purposes. Open-celled metal foams, however, can be used to *enhance* heat transfer in applications such as cryogenic heat exchangers, heat exchangers for airborne equipment, coal combustors [2], compact heat sinks for high power electronic devices [6], heat shielding for aircraft exhaust, compact heat exchangers [7], liquid heat exchangers [7, 8], air-cooled condenser-cooling towers and regenerators for thermal engines [4]. More uses of these relatively new materials are expected in the future, particularly because low density foams with remarkably uniform and regular cell morphologies are currently being developed using affordable processing methods.

Most of the previous studies on heat transfer in porous medium are based on Darcy's law which is only valid for creeping flows through an infinitely extended uniform medium with Reynolds numbers less than about 10 [2, 9]. Under such conditions, the fluid and the solid matrix may be assumed to be in local thermal equilibrium so that the fluid saturated porous medium can be treated as a continuum [7, 8, 10, 11]. This paper deals with direct-contact type heat exchangers (e.g. a porous channel bounded by isothermal or isoflux plates)

where the fluid velocity is high and the porous medium is bounded, rendering the assumption of Darcian flow and local thermodynamic equilibrium invalid. The objective is to obtain a functional relationship between the cellular structure and the heat-transfer characteristics for forced convective flows through open-celled metal foams. A simple cubic cell model consisting of slender cylinders as edges is developed to capture the most important behavioral trends of energy flow due to forced convection and conduction through cell ligaments of the cellular foam. Use is made of the analogy between flow through the foam and that across a bank of cylinders. The solid matrix and the convective fluid are treated separately by the model. Approximate closed-form solutions for the overall heat transfer coefficient and pressure drop as functions of cell morphologies and other relevant heat transfer parameters are obtained, which can be used to guide the design of optimum cellular structures that maximize the heat transfer rate per unit pumping power (the energy expended driving the convective flow). The model is applied to evaluate the heat transfer efficiency of open-celled foams as heat sinks for power electronic components, as well as the performance of air–fuel heat exchangers consisting of foam laminates.

It should be pointed out that the present model, which is based on crossflow across a bank of cylinders, has been idealized in several ways to limit the complexity of forced convective flow across an open-celled foam. Some of the simplifying assumptions made in order to analyze heat transfer in the disordered porous material likely lead to an overprediction of the actual level of heat transfer but nevertheless should capture the approximate functional dependence of the different control variables such as foam density, cell size and fluid velocity [2].

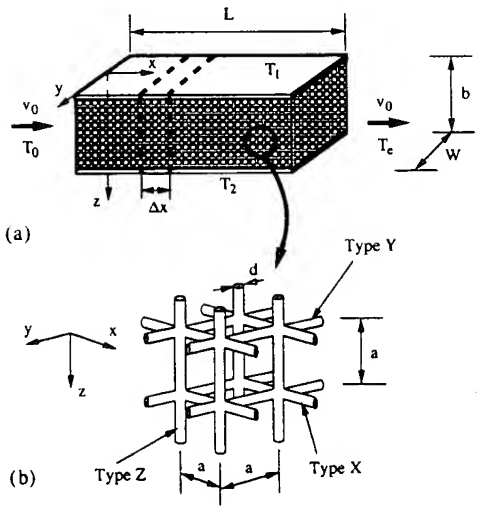

Fig. 1. Open-celled foam under forced convection: (a) notations, (b) cubic unit cell.

2. SPECIFICATION OF THE MODEL

Referring to Fig. 1(a), we consider the *steady-state* heat flow in an open-celled foam made up of uniform distributed, equal-sized cubic cells, sandwiched between two plates of length L and width W. The cubic unit cell is chosen for its simplicity, allowing for approximate closed-form solutions for important heat transfer parameters. The dimensions of the cell are chosen such that the surface area density of the model foam equals that of the real foam which can be measured accurately by using a micro-computed-tomography system [2]. Both plates are assumed to be thin and have large thermal conductivity so that the through-thickness heat conduction may be neglected; thus, uniform temperatures T_1 and T_2 are prescribed, respectively, on the top ($z = 0$) and bottom ($z = b$) plates. Without loss of generality, it is assumed that $T_1 \geq T_2$, and that the sandwich structure is capped and thermally insulated at both ends $y = W/2$ and $y = -W/2$. Cooling fluid, velocity v_0, temperature T_0 ($< T_2$) and pressure p_0, is forced into the foam at $x = 0$ (the inlet) and exits at $x = L$ (the outlet) with temperature T_e and pressure p_e. The simple cubic unit cell shown in Fig. 1(b) is taken as consisting of three mutually perpendicular equivalent cylinders, each having diameter d, length a and thermal conductivity λ_s. For simplicity, the cylinders making up the cell edges are assumed to be each parallel to the x-, y- or z-coordinate and referred to hereafter as cylinders X, Y and Z, respectively. Thus, the flow of fluid is normal to cylinders of both types Y and Z, but parallel to type X (Fig. 1). The cell size a is assumed to be much smaller than the plate width W so that heat transfer in each cell envisioned in Fig. 1 is assumed to be independent of y. The design objective is to obtain the maximum heat transfer per unit pumping power from the sandwich system.

The model presented in Fig. 1 is analyzed in three steps. We start in Section 3 by calculating the heat transfer from a single cylinder of type Z and length b, with temperature T_1 specified on its top and T_2 at its bottom (Fig. 2(a)). When T_2 is sufficiently low, heat is lost not only by convection to the fluid but also by conduction to the environment (through the lower plate). However, for higher T_2 or a larger heat transfer coefficient on the cylindrical surface, reverse flow of heat occurs at the bottom half of the cylinder, so that heat is extracted from both the lower plate and the upper one into the cylinder. The condition governing such reverse flow of heat is obtained. These results are then extended in Section 4 to analyze a bank of parallel, unconnected cylinders of type Z in cross-flow, arranged in a square array in the (x, y)-plane. Expressions for the average heat transfer coefficient, average fluid temperature inside the array, and total heat transfer from the system are obtained. The problem specified in Fig. 1 is solved in Section 5,

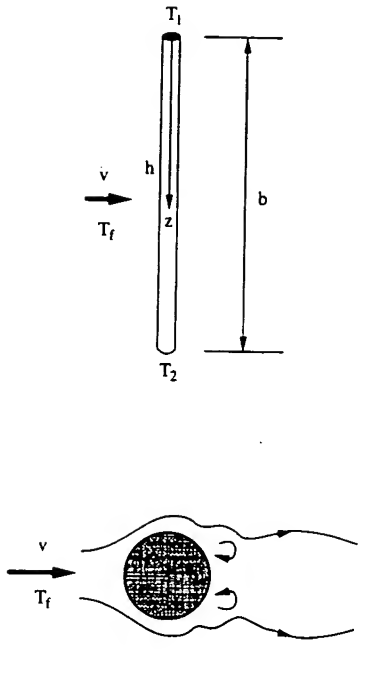

Fig. 2. Single cylinder in cross-flow: (a) longitudinal view, (b) cross-sectional view.

based on solutions described above. The surface area density of the model foam is calculated and compared to the data provided by ERG (Energy Research and Generation) for their Duocel® aluminum foam, as well as data for other types of heat exchangers. The overall heat transfer coefficient and pressure drop caused as the fluid flows across the foam are calculated using the model and the optimum foam properties for the best heat transfer performance are suggested. Finally, two examples of practical importance are presented in Section 6: compact multi-chip modules having convectively cooled foams as heat sinks, and multi-layered heat exchangers where heat transferred from one flowing fluid to another is substantially enhanced by the use of foams.

3. A SINGLE CYLINDER IN CROSS-FLOW

The metal ligaments in an open-celled foam are similar in many ways to fins common in heat exchangers so we begin by considering a single, isolated cylinder of type Z, originally situated at (x, y) in the sandwich structure (Fig. 2). The average temperature of the fluid flowing across the cylinder, T_f, depends on the position of the cylinder in the direction of flow (x-direction), but is here assumed to be independent of z. (The validity of this assumption and its limitation is discussed in Section 5.2, whereas the x-dependence of T_f is treated in Section 4.2.) Let h be the average heat transfer coefficient associated with the cylinder subjected to cross flow. The cylinder is considered to be slender ($d \ll a < b$) so that its temperature, $T(z)$, is uniform across the cylinder which allows for a simple closed-form solution for $T(z)$. This simplification stems from the observation that the aspect ratio d/a is typically small for most low-density, open-celled metal foams (Duocel® Al foams, for instance, have an aspect ratio ranging from 0.1 to 0.2, see Fig. 4).

3.1. Temperature field and heat transfer

A standard "fin" analysis is useful for characterization of the metal ligaments. Under steady-state conditions, the variation of temperature T along the length of a slender cylinder is governed by [13]

$$\frac{d^2T}{dz^2} - \frac{4h}{\lambda_s d}(T - T_f) = 0 \tag{3.1}$$

where the Fourier law of heat conduction and Newton's law of cooling have been used. For typical uses of metal foams, heat transfer due to radiation at the cylindrical surface is usually at least one order of magnitude smaller than that due to forced convection (Appendix A), so it will be neglected. The solution to equation (3.1), with the boundary conditions that at $T = T_2$ $z = 0$ and at $T_1 = T_2$ $z = b$, is

$$T(z) = T_f + \frac{(T_1 - T_f)\sinh[2\mathrm{Bi}^{1/2}(b - z)/d] + (T_2 - T_f)\sinh(2\mathrm{Bi}^{1/2}z/d)}{\sinh(2\mathrm{Bi}^{1/2}z/d)} \tag{3.2}$$

where $\mathrm{Bi} = hd/\lambda_s$ is the Biot number. The average temperature of the cylinder, $\bar{T}$, is therefore

$$\bar{T} = T_f + (T_1 + T_2 - 2T_f)\frac{\cosh(2\mathrm{Bi}^{1/2}b/d) - 1}{(2\mathrm{Bi}^{1/2}b/d)\sinh(2Bi^{1/2}b/d)} \tag{3.3}$$

which has a lower bound $\bar{T} = T_f$ when $\mathrm{Bi} \to \infty$ (convection dominated) and an upper bound $\bar{T} = (T_1 + T_2)/2$ at $\mathrm{Bi} = 0$ (insulated cylinder). In most applications involving air and water cooling, $h \sim 10^2$–10^4 W/(m^{2}K), $d \sim 10^{-4}$ m and $k \sim 10^2$ W/(m K) rendering $\mathrm{Bi} \ll 1$, such that $(T_1 + T_2)/2$ is a good estimate for $\bar{T}$. Equation (3.2) dictates that a thermal boundary layer with thickness $O(\mathrm{Bi}^{1/2}d)$ exists near both ends of the cylinder for the high Bi regime. The temperature is more uniform away from the ends, approaching T_f for $\mathrm{Bi} > 0.02$. In general, $\bar{T} \approx (T_1 + T_2)/2$ if $\mathrm{Bi} < 0.002$ whilst $\bar{T} \approx T_f$ when $\mathrm{Bi} > 0.02$.

The heat flux entering the cylinder at $z = 0$, $q = -(\pi d^2/4)\lambda_s(dT/dz)_{z=0}$, follows from equation (3.2) as

$$q = (\pi/2)\lambda_s \mathrm{Bi}^{1/2} d \frac{(T_1 - T_f)\cosh(2\mathrm{Bi}^{1/2}b/d) - (T_2 - T_f)}{\sinh(2\mathrm{Bi}^{1/2}b/d)} \tag{3.4a}$$

whereas the loss of heat at the end of the cylinder due to conduction through the solid, $q_c = -(\pi d^2/4)\lambda_s(dT/dz)_{z=b}$, is given by

$$q_c = (\pi/2)\lambda_s \mathrm{Bi}^{1/2} d \cdot \times \frac{(T_1 - T_f) - (T_2 - T_f)\cosh(2\mathrm{Bi}^{1/2} b/d)}{\sinh(2\mathrm{Bi}^{1/2} b/d)} \quad (3.4b)$$

The heat carried away by the cooling fluid, q_h, is obtained by subtracting q_c from q, yielding

$$q_h = (\pi/2)\lambda_s \mathrm{Bi}^{1/2} d(T_1 + T_2 - 2T_f)\tanh(2\mathrm{Bi}^{1/2} b/d) \quad (3.4c)$$

However, depending on the magnitude of the Biot number Bi, q_c of equation (3.4b) may be negative, as exploited below, owing to the competition between conductive loss at $z = b$ ($T_1 > T_2$) and positive conductive flux ($T_2 > T_f$).

3.2. Condition for reverse flow of heat

In the limit when the cylinder is insulated, equations (3.4a)–(c) reduce to

$$q = q_c = (\pi d^2/4)\lambda_s(T_1 - T_2)/b, \quad q_h = 0 \quad (3.5)$$

In the limit $\mathrm{Bi} \to \infty$ when convective transport is dominant,

$$q_c/q = -(T_2 - T_f)/(T_1 - T_f), \quad q_h/q = (T_1 + T_2 - 2T_f)/(T_1 - T_f), \quad (3.6)$$

so that, with $T_f \le T_2 \le T_1$, reverse flow of heat occurs at the lower half of the cylinder, $q_c = -q$ and $q_h = 2q$ if $T_1 = T_2$. For finite Bi, heat flux into the system from the lower boundary at $z = b$ occurs when $\mathrm{Bi} > \mathrm{Bi}^*$ where

$$\mathrm{Bi}^* = \left(\frac{d}{b}\right)^2 \cosh^{-2}\left(\frac{T_1 - T_f}{T_2 - T_f}\right) \quad (3.7)$$

It is clear that energy flows into the cylinder from both ends if $T_f \le T_2 = T_1$, i.e. $\mathrm{Bi}^* = 0$. Thus, the total transfer of energy to the fluid from the single cylinder system, $\bar{q}$, is

$$\bar{q} = \begin{cases} q & \text{if } \mathrm{Bi} \le \mathrm{Bi}^* \\ q_h & \text{if } \mathrm{Bi} \ge \mathrm{Bi}^* \end{cases} \quad (3.8)$$

As an illustration, given $(T_1 - T_f)/(T_2 - T_f) = 2$, $\lambda_s = 200$ W/(m K), $d = 0.5$ mm and $b = 100d$, the heat transfer coefficient h must be larger than 10 W/(m^2 K) if reverse flow of heat is to occur at the bottom of the cylinder.

4. A BANK OF TYPE Z CYLINDERS IN CROSS FLOW

In this section, the results obtained above for a single cylinder of type Z are applied to study a simplified version of the sandwich structure shown in Fig. 1(a) where the fluid passes a bank of type Z cylinders, squarely arranged in the (x, y) plane but *unconnected* by cylinders of either type X or Y. The effects of these connecting struts constitute the subject treated in Section 5.

4.1. Heat transfer coefficient h

The transfer of energy due to high-Reynolds-number streaming flow past a heated single cylinder or a bank of heated cylinders has been a subject area of enormous studies, but results are largely limited to empirical correlations. For most practical applications, dimensional analysis of the heat transfer processes suggests that the Nusselt number, $\mathrm{Nu} = hd/\lambda_f$, is a function of the Reynolds number, $\mathrm{Re} = vd/\nu_f$, and the Prandtl number, $\mathrm{Pr} = c_p\mu_f/\lambda_f$. Here, v is the average velocity of the fluid far from the cylinder, and λ_f, ν_f, μ_f and c_p stand for the thermal conductivity, kinematic viscosity, shear viscosity and specific heat (at constant pressure) of the fluid, respectively, all evaluated at the *film temperature* (the arithmetic mean between the surface and free-stream temperatures). The Nusselt number Nu may be interpreted as the ratio of the actual heat transfer coefficient h to the conductive heat transfer coefficient λ_f/d of the fluid. The Prandtl number Pr is the ratio of the kinematic viscosity to the thermal diffusivity, measuring the relative efficiency of the fluid as a conductor of momentum and energy. The Reynolds number Re measures the ratio of inertial forces to viscous forces in the flow. Consequently, the overall heat transfer coefficient is expected to increase as the Reynolds number or Prandtl number, or both, increase.

According to Gosse [14], for a single cylinder in cross flow (Fig. 2(b)) and $\mathrm{Re} > 40$, the *local* Nusselt number at the front face ($0 \le \phi \le 4\pi/9$) can be expressed as

$$\mathrm{N}(\phi) \equiv h(\phi)d/\lambda_f = 1.05(1 - \phi^3)\mathrm{Pr}^{1/3}\mathrm{Re}^{1/2}$$

Heat transfer due to convection at the back face ($4\pi/9 \le \phi \le \pi$) is relatively small for small Re numbers ($\mathrm{Re} < 40$), but may exceeds that at the front face when Re becomes large. The *average* Nusselt number for the whole cylinder may then be described in the form

$$\mathrm{Nu} = C\mathrm{Pr}^{1/3}\mathrm{Re}^n, \quad (4.1)$$

where C and n are dimensionless constants which has been found to be appropriate for most ordinary gases and liquids, except for liquid metals [9, 15, 16]. This expression is also useful for non-cylindrical shapes of objects, subjected to changes in (C, n) and the replacing of d by the hydraulic diameter d_H.

For a bank of parallel but unconnected cylinders subjected to cross-flow, heat transfer is still governed by the Nusselt number expressed in the form of equation (4.1) such that the overall heat transfer coefficient *averaged* over all the cylindrical surfaces may be described by [16, 17]

$$h = \lambda_f C \mathrm{Pr}^{1/3} (v_{max}/\nu_f)^n d^{n-1} \quad (4.2)$$

Here, v_{max} is the maximum fluid velocity occurring in the bank, and (C, n) are dependent on the Reynolds number and the geometric characteristics (e.g. relative spacing of the cylinders, numbers of rows of cylinders, and the flow direction). Equation (4.2) has been correlated with extensive experimental data for both gases and liquids and for a number of in-plane arrangements of cylinders [16, 18–20]. For cylinders arranged in a square array with at least 10 rows in each direction such that a repeatable pattern of flow is established inside the bank, $C \approx 0.3$ and $n \approx 0.6$ when $a/d \geq 3$, rendering $h \propto d^{-0.4}$ [16, 17]. For air at atmospheric pressure and room temperature with $v_{max} = 1$ m/s and for a bank of cylinders having diameter $d = 0.5$ mm, one calculates from equation (4.2) that $h \approx 150$ W/(m^2 K). If air is replaced by water with other geometric and flow conditions unchanged, $h \approx 4 \times 10^4$ W/(m^2 K).

Using the properties tabulated in Holman [16] for common fluids (e.g. air and saturated water), we find that the heat transfer coefficient h depend weakly on temperature. Therefore, the temperature dependence of h is neglected in the analysis below.

4.2. Fluid temperature

The temperature of the cooling fluid increases continuously as it flows along the bank of cylinders and so the driving force for heat transfer is continually diminished. We therefore wish to establish the fluid temperature as a function of downstream position x, the plate temperatures (T_1, T_2) and the properties of the foam.

It is not attempted below to find the detailed temperature field of the fluid everywhere in the bank, given the turbulent flow and limited information on the heat transfer coefficient. Instead, several simplifications are made to arrive at an approximate solution for the steady-state temperature distribution of the fluid inside the bank. For simplicity, the lower plate temperature T_2 is set equal to T_1 although this restraint can be relaxed if necessary. We assume that heat transfer between the fluid and the plates is governed by the same coefficient h for cross-flow over cylinders, namely equation (4.2). We further assume that the turbulent flow inside the foam is well mixed and so develop a one-dimensional model for the fluid temperature, T_f, with the variations of T_f with z (and y) neglected. This is partially supported by the result of Kaviany [9] on the fully-developed flow through a porous channel bounded by isothermal parallel plates (Fig. 1):

$$\frac{v(z)}{v_0} = \frac{1 - e^{-2\gamma} - (1 - e^{-\gamma})[e^{\gamma(z/b-1)} + e^{-\gamma z/b}]}{1 - e^{-2\gamma} - 2(1 - e^{-\gamma})^2 \gamma^{-1}}$$

where $\gamma = (b^2\varepsilon/K)^{1/2}$ is the porous medium shape parameter, K being the permeability of the porous medium and ε the porosity. There is a strong dependence of the fully-developed velocity profile $v(z)$ on γ; as γ increases, the central region containing a uniform velocity distribution spreads further toward the plates, with the velocity variation confined to a very thin layer adjacent to the plates at large γ. Also, by dimensional analysis, Vafai and Tien [11] showed that the boundary-layer thickness is of the order of γ^{-1}. Notice that for a duct filled with metal foam, the typical values of γ range from 10^1 to 10^3.

Consider an arbitrary slice of the sandwich structure located at x with length Δx (Fig. 1(a)). With $N_s = \Delta x/a^2$ denoting the total number of cylinders inside the slice per unit thickness, the loss of heat from the cylinders to the streaming fluid is N_s times that from a single cylinder, q_h, given by equation (3.4c). An energy balance on the sliced structure shown in Fig. 1(a) gives

$$\dot{m} c_p [T_f(x + \Delta x) - T_f(x)] = N_s q_h + q_w \quad (4.3)$$

where $\dot{m} = \rho_f v_f b$ is the mass flow rate per unit width at the entrance to the bank and ρ_f is the fluid density at the entrance. Also, q_w is the heat flux into the fluid from both plates over length Δx and unit width,

$$q_w = (2\eta \Delta x) h [T_1 - T_f(x)] \quad (4.4)$$

where

$$\eta = 1 - \pi d^2/4a^2 \quad (4.5)$$

is the net surface area of the plate per unit length per unit width excluding the cross-section areas of the N_s cylinders. Combining equation (4.3) with equations (4.4) and (3.4c) (with $T_1 = T_2$) results in

$$\frac{T_f(x + \Delta x) - T_f(x)}{T_1 - T_f(x)} = (\Delta x) \frac{2\eta h}{\rho_f c_p v_f b} \times \left[1 + \frac{\pi}{2\eta \mathrm{Bi}^{1/2}} \left(\frac{d}{a}\right)^2 \tanh\left(\frac{2\mathrm{Bi}^{1/2} b}{d}\right)\right] \quad (4.6)$$

It follows immediately that the characteristic length scale l for fluid temperature variations in the direction of flow is given by

$$l = \frac{\rho_f c_p v_f b}{2\eta h} \left[1 + \frac{\pi}{2\eta \mathrm{Bi}^{1/2}} \left(\frac{d}{a}\right)^2 \tanh\left(\frac{2\mathrm{Bi}^{1/2} b}{d}\right)\right]^{-1} \quad (4.7)$$

In the limit $\Delta x \to 0$, equation (4.6) provides an ordinary differential equation for $T_f(x)$ which can be readily solved to obtain

$$T_f(x) = T_1 - (T_1 - T_0)\exp(-x/l) \quad (4.8)$$

The average of $T_f(x)$ over length L is

$$\bar{T}_f = T_0 + (T_1 - T_0)\left[1 - \frac{l}{L}\left(1 - \exp\left(-\frac{L}{l}\right)\right)\right] \quad (4.9)$$

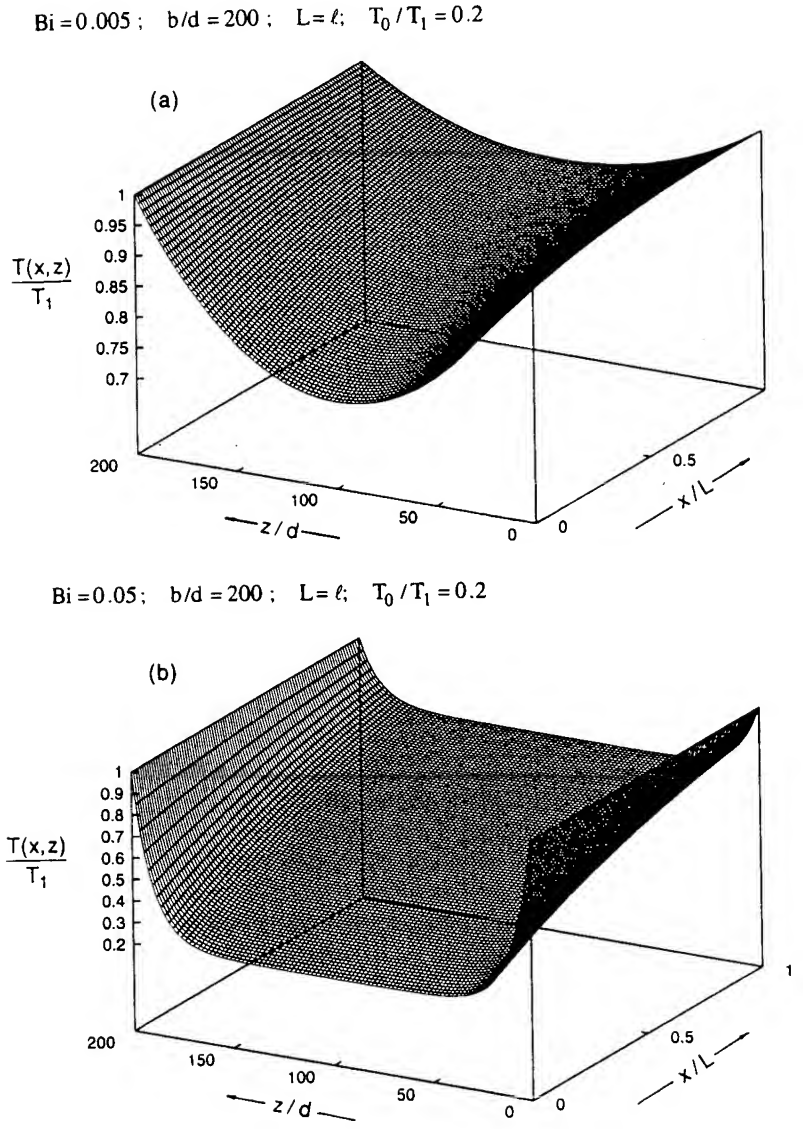

Fig. 3. Predicted foam temperature distribution for (a) $Bi^{1/2}=0.005$, (b) $Bi^{1/2}=0.05$ (with b/d = 200, $L = l$ and $T_0/T_1=0.2$).

The significance of equations (4.7), (4.8) and (4.9) will be discussed below in some detail regarding model foams with simple cubic cells. The temperature of each cylinder in the bank is obtained by substituting equation (4.8) into equation (3.2). As an illustration, Fig. 3 presents the distribution of the normalized cylinder temperature, $T(x, z)/T_1$, for $Bi^{1/2}$ = 0.005 and 0.05, respectively, with b/d = 200, $T_0/T_1=0.2$ and the foam length L chosen equal to the characteristic length scale l. Notice the presence of a boundary layer along the cylinders near the plate wall, which thickens as Bi decreases or x/L increases.

5. FOAMS WITH OPEN CUBIC CELLS

The analysis of heat transfer in the model foam structure thus far has ignored the contributions to heat transfer from type X and Y cylinders that connect cylinders of type Z. As illustrated schematically in Fig. 1(b), the three types of cylinders (which are assumed to have a high conductivity relative to that of the fluid), mutually perpendicular, are each arranged in a square array in their respective cross-planes and meet at three-way joints uniformly distributed inside the foam. Under *steady-state* flow conditions, the average temperature of type X and

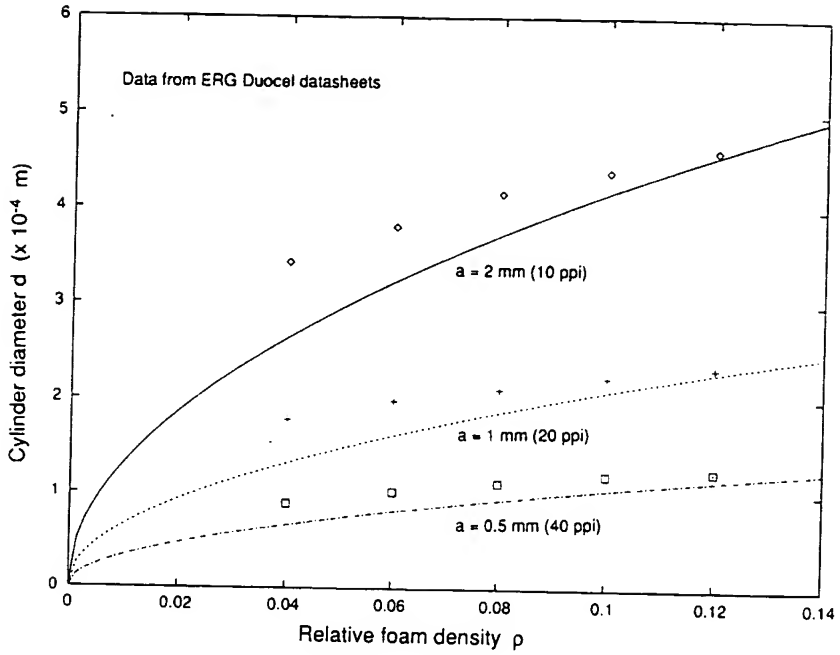

Fig. 4. Predicted cylinder diameter as a function of foam density compared with that measured for aluminum foam, for three cell sizes: a = 0.5, 1 and 2 mm.

Y cylinders inside a cell located at x is expected to be approximately the same as that of the type Z cylinder meeting them at the joint of the cell. Thus, all the cylinders in a single slice of the structure shown in Fig. 1(a) may be assumed to have an average temperature $\bar{T}(x)$, coupled to the average fluid temperature $\bar{T}_f(x)$ through equation (3.3). It follows that type Y cylinders, subjected to cross flow, have the same average heat transfer coefficient h as that given by equation (4.2) for type Z cylinders, also under cross flow. On the other hand, although the average heat transfer coefficient for type X cylinders under longitudinal flow is still described in a form similar to that given in equation (4.2), extra terms need to be introduced to account for the dependence on the cylinder length [14]. Such dependence is nonetheless assumed to be fairly weak when $x > 10a$ (see discussion below) where the flow pattern is well established. For simplicity and also due to the lack of more detailed data on longitudinal flow over a bank of cylinders, it is assumed below that type X cylinders are characterized by the average heat transfer coefficient of equation (4.2). Under these assumptions, the solution obtained in Section 4 for a bank of type Z cylinders applies as well to the model foam structure of Fig. 1(a), with due account of the extra number provided by type X and Y cylinders plus their contributions to the total surface area for heat transfer.

5.1. *Cylinder diameter and surface area density*

For an open cubic cell consisting of *slender* cylinders, the diameter of the cylinder is approximately related to the relative foam density, ρ, by

$$\frac{d}{a} \approx \left(\frac{2}{\sqrt{3\pi}}\right)\rho^{1/2} \tag{5.1}$$

where a is the cell size and $\rho \equiv \rho^*/\rho_s$, with ρ^* denoting the foam density and ρ_s the density of the solid. The resulting total surface area A per unit width (in the y-direction) of a segment of foam of height b and length L, is approximately

$$A \approx \left(\frac{2\sqrt{3\pi}Lb}{a}\right)\rho^{1/2} \tag{5.2}$$

The surface area density, $\alpha_A \equiv A/V$ with V denoting the volume of the foam, is an important parameter for the heat exchange systems:

$$\alpha_A \approx \left(\frac{2\sqrt{3\pi}}{a}\right)\rho^{1/2} \tag{5.3}$$

The predicted cylinder diameter, d, from equation (5.1) is plotted on Fig. 4 as a function of relative foam density, ρ, for three values of cell size, a = 0.5, 1.0 and 2.0 mm. The ERG data for Duocel® Al foam are also included, corresponding to cell sizes of 10, 20 and 40 ppi (pores per inch), respectively. The mean cell size for these foams,

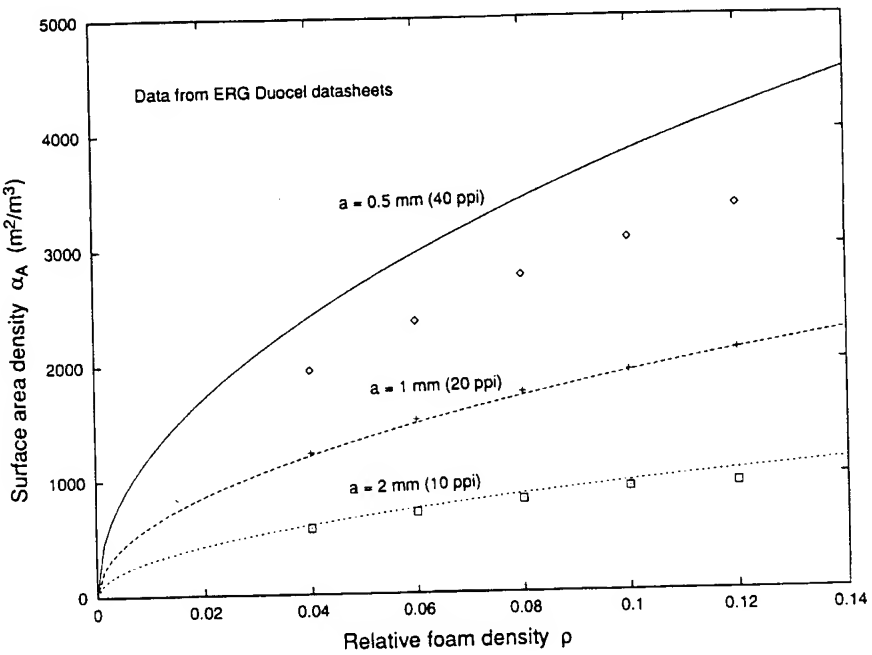

Fig. 5. Predicted surface area density as a function of foam density compared with that measured for aluminum foam, for three cell sizes: a = 0.5, 1 and 2 mm.

according to the ERG catalogue, are 2.0, 1.0 and 0.5 mm, respectively. The simple cubic cell model is seen to be fairly representative, bearing in mind that for a given ppi, the nominal cell size of a real foam is not constant but dependent upon ρ, and also that the cell ligaments of the ERG foams are best described as a rod with rectangular or triangular cross-section rather than a circular cylinder.

In Fig. 5, the surface area density, α_A, calculated from equation (5.3) is plotted as a function of ρ with a = 0.5, 1.0 and 2.0 mm, respectively. Again, the model correlates well with the ERG data. In the 40 ppi case, however, a 25% difference between the prediction and measurement is present which may be attributed to the actual mean cell size being different from the nominal mean cell size used in the calculation, a = 0.5 mm. (Microstructural characterizations suggest that the Duocel® foam labelled by ERG as 40 ppi is actually described more closely by 30 ppi.) With $\alpha_A > 1000$ m^2/m^3 even at very low densities ($\rho \approx 0.02$), the conclusion drawn from these results is that open-celled metal foams well qualify as compact heat exchangers. Compact heat exchanger generally require $\alpha_A > 700$ m^2/m^3 [9, 21] and are essential in applications where the size and weight of the heat exchanger is constrained due to design considerations (e.g. automobiles, airborne equipments and air conditioners). For comparison, automotive radiators have $\alpha_A \approx 600$–1000 m^2/m^3, cryogenic heat exchangers 1000–2000 m^2/m^3, gas turbine rotary regenerators 3000–6000 m^2/m^3, and human lungs 10^4 m^2/m^3 [21].

5.2. Characteristic length scales

5.2.1. Minimum flow length l_1. As shown in Fig. 6, two length scales are of importance to the present design problem: the length l_1 the fluid must travel to raise its temperature from T_0 to the goal temperature T_G (which is fixed by the plate temperature T_1), and the distance l_2 from the inlet at which the bulk of the fluid attains a fully mixed state with uniform temperature and velocity except in a region of thickness δ adjacent to the plate. Practically, l_1 may serve as a guideline for selecting the total length L of the sandwich structure to achieve the targeted fluid temperature at the duct exit, whereas l_2 dictates the range within which the current model is valid.

Consider first the characteristic length scale l_1 for fluid flow. From its definition above and equation (4.8), it is related to the length scale l for fluid temperature changes (equation (4.7)) via

$$l_1 = l \ln\left(\frac{1 - T_0/T_1}{1 - T_G/T_1}\right) \tag{5.4}$$

Since each cubic cell effectively contains one cylinder of each type (assuming $a/d > 3$), the total number of cylinders, N_s, inside a slice of length Δx and unit width, now becomes

$$N_s = \frac{3\Delta x}{a^2} \tag{5.5}$$

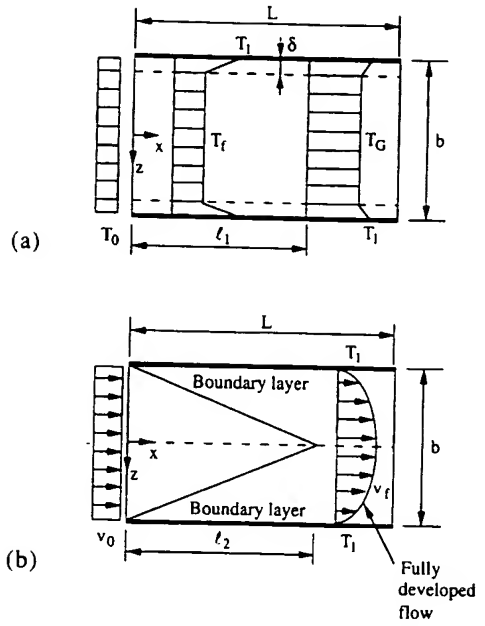

Fig. 6. Characteristic length scales of heat transfer in a duct filled with open-celled foam: (a) temperature profile, (b) velocity profile.

Since the second term in the bracket on the right side of equation (4.7) has a typical value of at least 10, l can be rewritten as

$$l \approx \frac{\rho_f c_p v_f b}{3\pi\lambda_s \mathrm{Bi}^{1/2}} \frac{a/d}{\tanh(2\mathrm{Bi}^{1/2} b/d)} \tag{5.6}$$

For consistency, one needs to check if at $x = l_1$ the average cylinder temperature $\bar{T}(l_1)$ still exceeds T_G. From equations (3.3) and (4.8), the average temperature of the cylinders as a function of x is obtained as

$$\frac{\bar{T}}{T_1} = 1 - \left(1 - \frac{T_0}{T_1}\right)\left[1 - \frac{\cosh(2\mathrm{Bi}^{1/2} b/d) - 1}{(\mathrm{Bi}^{1/2} b/d)\sinh(2\mathrm{Bi}^{1/2} b/d)}\right] \times \exp(-x/l) \tag{5.7}$$

It follows that

$$\bar{T}(l_1) = T_G + \frac{\cosh(2\mathrm{Bi}^{1/2} b/d) - 1}{(\mathrm{Bi}^{1/2} b/d)\sinh(2\mathrm{Bi}^{1/2} b/d)}(T_1 - T_G) \tag{5.8}$$

which is larger than T_G as long as $T_G < T_1$.

Selected calculations for air reveal that, for relatively large foam densities ($\rho > 0.2$), the normalized *minimum flow length* l_1/a increases sharply as the normalized foam thickness b/a increases, becoming linear in b/a when b/a is larger than about 10. On the other hand, l_1/a is nearly independent of ρ when the foam is reasonably thick ($b/a > 10$). In addition, it has been verified that l_1/a decreases as the Biot number Bi is increased.

5.2.2. Thermal entrance length l_2. By definition, the thermal entrance length, l_2, is the longitudinal length from the inlet to the location where the thermal boundary layer becomes as thick as the duct itself. In contrast to the thermal entrance region ($x < l_2$) where the shape of the transversal temperature profile changes from one location to the next, in the thermally fully developed region ($x > l_2$), the shape (although not the amplitude) of the temperature profile is preserved. It is expected that the thermal entrance length is closely related to the hydraulic entrance length l_2' (i.e. the longitudinal distance at which the center-line velocity is 99% of its value for a fully developed field). Compared with the other characteristic length scale l_1, the length l_2 is more difficult to calculate owing to the complex and unsteady nature of fluid flow in the entry region. A rough estimate of l_2 is attempted below.

Consider the entry region to the duct as shown in Fig. 6. If the duct is not filled with foams, it has been established [22] that the thermal entrance length under laminar flow conditions is approximately given by

$$l_2/b \approx 0.05 \mathrm{Re}_b \mathrm{Pr} \tag{5.9a}$$

which is of the same order of magnitude as the hydraulic entrance length l_2' for fluids with $\mathrm{Pr} \approx 1$ (e.g. air): If l_2' is negligible relative to b, then l_2 is also negligible [10]. When the Reynolds number $\mathrm{Re}_b = v_f b/\nu_f$ has a value larger than about 2000 [15, 16], turbulent flow prevails in the duct, resulting in [16]

$$l_2/b = 50 \tag{5.9b}$$

For a duct filled with open-celled foam subjected to convective flows with $Re_b > 2000$, the fluid flow is expected to be more turbulent and unstable once it enters the duct because of the large disturbances caused by the presence of numerous foam cells and their torturous ligaments. In addition, the roughness of the plate surfaces due to the foam attachments is expected to dominate the turbulent motion in the boundary layer adjacent to the duct wall. Hence, a smaller l_2/b than that given by equations (5.9a)–(b) is expected throughout the duct. Kaviany [8] found that the hydraulic entrance length l_2' decreases *rapidly* with an increase in the porous medium shape parameter $\gamma = (b^2\varepsilon/K)^{1/2}$ ($l_2' \propto \gamma^{-2}$ for flow over a plate in saturated porous media [11]). Thus, as $10^1 < \gamma < 10^3$ for a typical duct filled with metal foam, the hydraulic entrance length l_2' for the porous medium is much shorter than that for a nonporous medium and is generally negligible [8]. Similar trends are expected to hold for the thermal entrance length l_2.

5.3. Overall heat transfer coefficient $\bar{h}$

If the amount of heat transferred directly from the bounding plates of the duct to the fluid, q_w, is neglected based on the same argument as that leading to equation (5.6), the loss of heat from a single slice of foam, length Δx and unit width, would be N_s times that from a single cylinder: $Q_s = N_s q_h$. The combination of equations (3.4c), (5.1) and (5.5) then leads to

$$Q_s(x) = [2\sqrt{3\pi}\lambda_s \mathrm{Bi}^{1/2}\rho^{1/2}\tanh(2\mathrm{Bi}^{1/2}b/d)] \times [T_1 - T_f(x)](\Delta x/a) \tag{5.10}$$

The total heat transfer from the whole sandwich structure per unit width, $Q_s(x)$, is obtained by integrating over all the slices, yielding

$$\frac{Q}{\lambda_s(T_1 - T_0)} = (l/a)[1 - \exp(-L/l)] \times [2\sqrt{3\pi}\mathrm{Bi}^{1/2}\rho^{1/2}\tanh(2\mathrm{Bi}^{1/2}b/d)] \tag{5.11}$$

Substitution of equations (4.8), (5.1) and (5.6) into equation (5.11) results in

$$Q = \dot{m}c_p(T_e - T_0) \tag{5.12}$$

where T_e is the temperature of the fluid at the outlet $x = L$ (Fig. 1(a)), given by

$$T_e = T_1 - (T_1 - T_0)\exp(-L/l) \tag{5.13}$$

Obviously, the maximum amount of heat that the fluid can extract from the system is $Q_{max} = \dot{m}c_p(T_1 - T_0)$.

The overall heat transfer coefficient of a foam-filled duct, $\bar{h}$, may be defined as

$$Q = 2L\bar{h}(T_1 - \bar{T}_f) \tag{5.14a}$$

such that heat transfer from the system is equivalent to that carried away by a fluid of average temperature $\bar{T}_f$, which flows across a *foam-free* but otherwise identical duct with the same average heat transfer coefficient $\bar{h}$ at the wall. The factor 2 is needed in equation (5.14a) because the duct has two plates each of length L. A straightforward manipulation using equations (4.8) and (4.9) shows that the temperature difference, $T_1 - \bar{T}_f$, is the well-known *logarithmic mean temperature difference* [16], ΔT_m, namely

$$\Delta T_m = T_1 - \bar{T}_f = \frac{T_e - T_0}{\ln[(T_1 - T_0)/(T_1 - T_e)]} \tag{5.14b}$$

From equations (4.9), (5.11) and (5.14a)–(b), one has

$$\bar{h} = (2h\rho\mathrm{Bi}^{-1/2})\tanh(2\mathrm{Bi}^{1/2}b/d) \tag{5.15}$$

which, in the limit $\mathrm{Bi}^{1/2}b/d \ll 1$, reduces to

$$\bar{h} = (\alpha_A b/2)h, \qquad \mathrm{Bi}^{1/2}b/d \ll 1 \tag{5.16a}$$

In the other limit when $\mathrm{Bi}^{1/2}b/d > 2$ such that $\tanh(2\mathrm{Bi}^{1/2}b/d) \approx 1$,

$$h = (\alpha_A/2)\sqrt{h\lambda_s d}, \qquad \mathrm{Bi}^{1/2}b/d > 2 \tag{5.16b}$$

where α_A is the surface area density of the foam given in equation (5.3). Notice that $(\alpha_A b/2)2L = A$ is the total surface area of heat transfer in the foam per unit width. Equation (5.15) is in general agreement with the test data of Bastawros and Evans [1] on ERG foams, giving the correct functional dependence of $\bar{h}$ on the fundamental variables (foam density, channel width, fluid velocity, etc.). However, the predicted value of $\bar{h}$ from equation (5.15) is much larger than that measured: At high air velocities ($v_f > 1$ m/s), the model predicts a typical $10 \sim 20$-fold increase in $\bar{h}$ if an empty duct is filled with an ERG foam; a $3 \sim$ five-fold increase of $\bar{h}$ is measured in stead. The overestimates may be attributed to the simplifying assumptions of the model in order to obtain simple analytical solutions to the difficult, relatively unstudied problem. On the other hand, the test set-up of Bastawros and Evans [2] is not quite the same as that shown in Fig. 1 and it is not clear if the forced air flow has a uniform velocity before and after it enters the foam (which is assumed to be the case in the model). Obviously, more measurements are needed to further check the validity and accuracy of the model predictions.

In analogy to standard duct flow problems, an average Nusselt number for the foam-filled duct system, $\overline{Nu}$, may be defined by [16]

$$\overline{Nu} = \bar{h}D/\lambda_f \tag{5.17a}$$

where D is the hydraulic diameter,

$$D = 4 \times \frac{\text{Cross-sectional area of fluid flow}}{\text{wetted perimeter of channel}}$$

$$= 4(1-\rho)/\alpha_A \tag{5.17b}$$

In lieu of equations (4.1), (5.15) and (5.17b), $\overline{\mathrm{Nu}}$ can be recast into the more familiar form

$$\overline{\mathrm{Nu}} = \bar{C}\mathrm{Pr}^{1/3}\mathrm{Re}^{n} \tag{5.17c}$$

where $\bar{C} = C(4\rho\mathrm{Bi}^{-1/2}D/d)\tanh(\mathrm{Bi}^{1/2}b/d)$. Often, the local Reynolds number Re in equation (5.17c) is replaced by $\mathrm{Re}_D = v_f D/\nu_f$.

5.4. Pressure drop

The pressure drop experienced by the cross-flow over a bank of squarely-arranged, parallel yet unconnecting cylinders may be expressed as [9, 16]

$$\Delta p = 2fN_L\rho_f v_{\max}^2 \tag{5.18}$$

where $N_L = L/a$ is the number of cylinder rows in

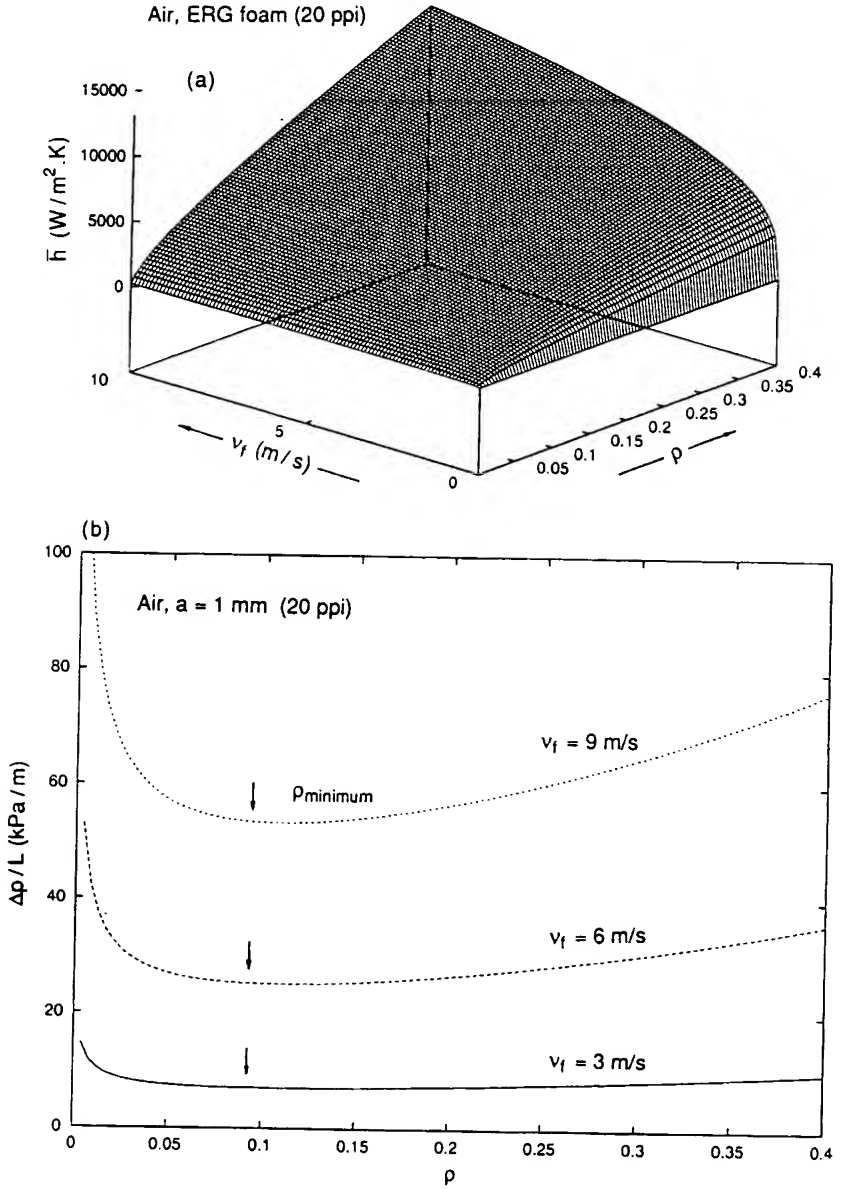

Fig. 7. Selected results on (a) overall heat transfer coefficient $\bar{h}$, (b) pressure drop per unit length $\Delta p/L$, as functions of relative foam density ρ and fluid velocity v_f for air (20°C) flowing across a duct filled with 20 ppi (a = 1 mm) ERG aluminum foam.

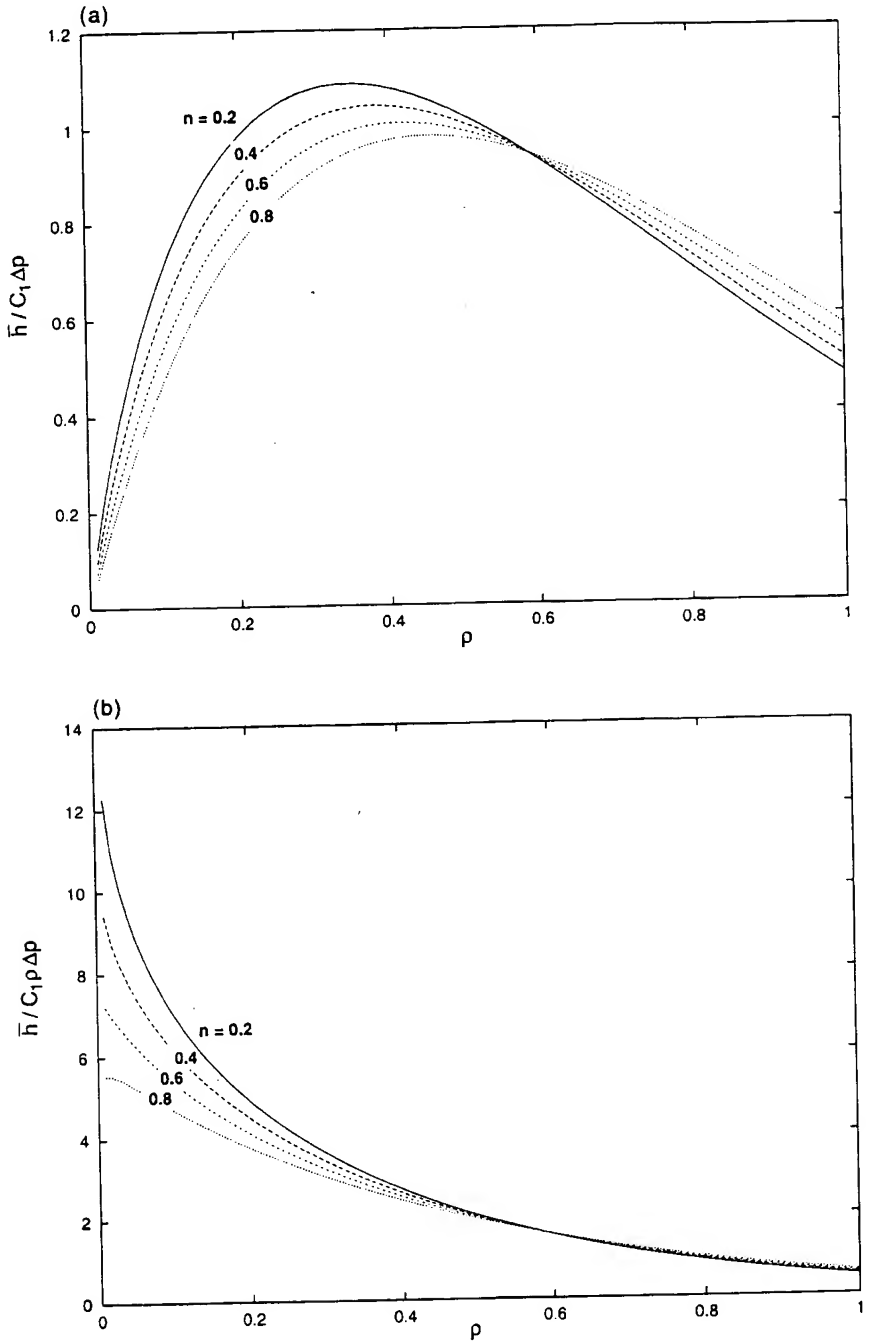

Fig. 8. Normalized foam performance indices, (a) I_1, (b) I_2, as functions of foam density for selected values of n.

the direction of flow and f is the friction factor. (The number of cylinders in the direction perpendicular to the flow is large so that Δp may be assumed uniform in the transverse direction.) For gases, f takes the following empirical relation [16, 23]

$$f = \left\{0.044 + \frac{0.008(a/d)}{(a/d-1)^{0.43+1.13(d/a)}}\right\} \mathrm{Re}_{\max}^{-0.15} \quad (5.19)$$

Here, $\mathrm{Re}_{\max} = v_{\max} d/\nu_f$ and $v_{\max} = v_f/(1 - d/a)$ is the maximum fluid velocity inside the bank. For gases

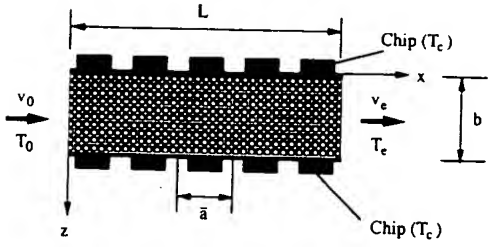

Fig. 9. Prototypical design of a compact multi-chip module cooled by forced convection through open-celled foam.

flowing across a foam with open cubic cells, the pressure differential produced by cylinders of type Y and Z may be approximated using equation (5.18) and equation (5.19) with $N_L = 2L/a$. The contribution to the pressure drop from type X cylinders and the plate surfaces is more complicated but the overall response of such an open-cell foam may be characterized by a frictional coefficient, χ, which is to be calibrated from experiment. In addition to the bulk frictional drag induced by the foam skeleton equation (5.18), the fluid flowing past a foam-filled duct also experiences a boundary frictional drag at the plate wall and a excess pressure loss at the entrance region. However, Kaviany [9] showed that the total pressure drop experienced by the flow across the foam-filled duct is dominated by the bulk frictional drag, hence

$$\Delta p = (4L/a) f \chi \rho_f v_{\max}^2 \qquad (5.20)$$

As a reference, the pressure drop of fully-developed laminar flows in a foam-free duct having length L and smooth surfaces is [16]

$$\Delta p = (12L/b)\rho_f v_f^2 / \mathrm{Re}_b \qquad (5.21)$$

where $\mathrm{Re}_b = v_f b/\nu_f$ and v_f is the mean flow velocity. Equations (5.19) and (5.20) suggest that $\Delta p \sim v_f^m a^{3-m}$ with $m = 1.85$ for foams having cubic unit cells. Experimental data on metal foams is scarce, but for open-celled ceramic foams it is found that m has a weak dependence on cell size, with $m = 1.82$, 1.88, 1.91 and 1.93 corresponding to foams of size 50, 30, 20 and 10 ppi, respectively [24]. For ERG foams, a smaller exponent ($m = 1.60$ both for 20 and 30 ppi foams) has been measured [13]. In general, the experimental data may be expressed using the quadratic interpolation [7]:

$$\frac{\Delta p}{L} = \frac{\mu_f}{K} v_f + \frac{\rho_f c_F}{K^{1/2}} v_f^2 \qquad (5.22)$$

to obtain the Forchheimer coefficient c_F and the permeability K. For creeping flows with low velocities, equation (5.22) reduces to Darcy's law.

5.5. *Optimum foam design*

Ideally, foams for many heat exchanger applications would simultaneously maximize the amount of heat transfer and minimize the pump power needed to force the fluid through. Using equation (4.2) and noticing that $\tanh(2\mathrm{Bi}^{1/2} b/d) \approx 1$

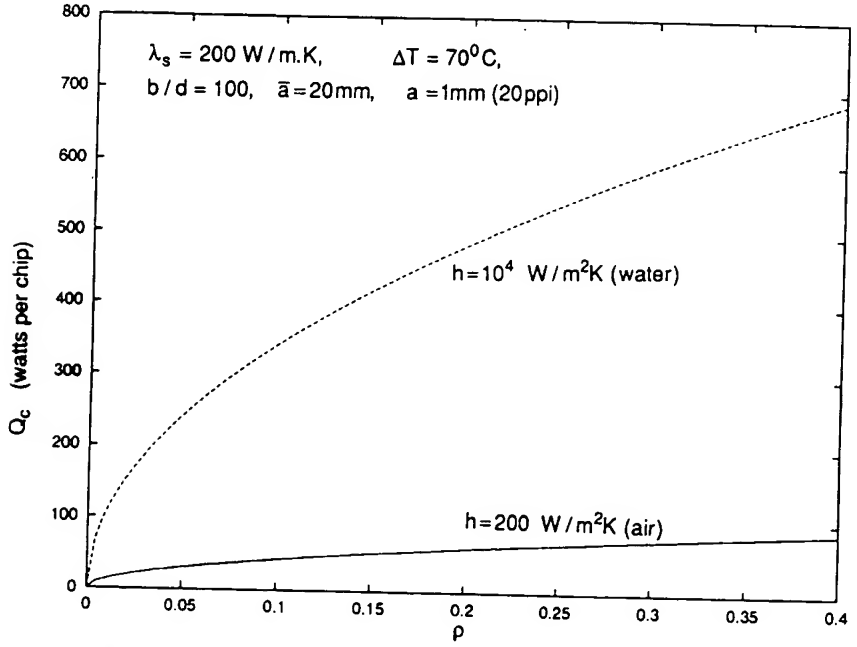

Fig. 10. Power dissipation per chip as a function of foam density for two types of cooling: air and water (with $v_f = 1$ m/s, $\Delta T = 70$°C, $\lambda_s = 200$ W/(m K), $a = 1$ mm, $\bar{a} = 2$ cm and $b/d = 100$).

in most applications, we can rewrite the overall heat transfer coefficient $\bar{h}$ of equation (5.15) in the form

$$\bar{h} = \sqrt{3\pi}\left(\frac{\lambda_s}{a}\right)\left(C\mathrm{Pr}^{1/3}\frac{\lambda_f}{\lambda_s}\right)^{1/2}\left(\frac{v_f a}{\nu_f}\right)^{n/2}\frac{\rho^{1/2}}{(a/d-1)^{n/2}} \tag{5.23}$$

where $C \approx 0.3$ and $n \approx 0.6$ if $a/d > 3$. Similarly, we can regroup the pressure drop Δp of equation (5.20) into

$$\Delta p = \left(\frac{4L\chi\rho_f v_f^2}{a}\right)\left(\frac{v_f a}{\nu_f}\right)^{-0.15}\frac{(a/d-1)^{0.15}}{(1-d/a)^2} \times \left\{0.044 + \frac{0.08(a/d)}{(a/d-1)^{0.43+1.13(d/a)}}\right\} \tag{5.24}$$

where it is assumed that χ is independent of a/d. The predicted overall heat transfer coefficient, $\bar{h}$, and pressure drop per unit length, $\Delta p/L$, are plotted on Fig. 7 as functions of relative foam density ρ and fluid velocity v_f for air at 20°C flowing across a duct filled with 20 ppi (a = 1 mm) ERG aluminum foam. These results are generally in agreement with the measurements by Schlegel *et al.* [24] on a ceramic foam except that its overall heat transfer coefficient is two orders of magnitude smaller than that of an ERG metal foam.

Whilst a foam having the smallest cell size and highest relative density maximizes heat transfer, it unfortunately also maximizes pressure drop (Fig. 7(b)). The predicted minimum pressure drop occurs at a relative density roughly equal to 0.09 for ERG foams, which is close to that measured by ERG. The heat transfer performance of the foam may be best characterized by a non-dimensional index I_1 combining both $\bar{h}$ and Δp, namely,

$$I_1 \equiv \frac{\bar{h}}{C_1 \Delta p} \tag{5.25a}$$

which, from equations (5.15) and (5.24), becomes

$$I_1 = \rho^{1/2}\frac{(1-d/a)^2}{(a/d-1)^{n/2+0.15}} \times \left\{0.044 + \frac{0.08(a/d)}{(a/d-1)^{0.43+1.13(d/a)}}\right\}^{-1} \tag{5.25b}$$

where C_1 is a parameter (with dimensions) independent of relative foam density, given by

$$C_1 = \left(\frac{\sqrt{3\pi}}{4}\right)\left(\frac{v_f a}{\nu_f}\right)^{n/2+0.15}\frac{(\lambda_s/L)(C\mathrm{Pr}^{1/3}\lambda_f/\lambda_s)^{1/2}}{\rho_f v_f^2} \tag{5.26}$$

For selected values of n Fig. 8(a) plots the index of foam performance, I_1C_1, as a function of relative foam density ρ. Clearly, there exists an optimum foam density, ρ_{optimum}, which would maximize I_1C_1. The value of ρ_{optimum} slightly increases as n is increased, but generally falls in the range $0.35 \sim 0.4$. The cell size, a, does not affect ρ_{optimum} as well as the behavior trend shown in Fig. 8 but, at a given density, foams with larger cell sizes perform better than those having smaller cells in size ($I_1 \sim a^{n/2+0.15}$). The experimental measurements of Schlegel *et al.* [24] on open-celled ceramic foams appear to support this latter conclusion. The optimal spacing of parallel plates or cylinders in forced convection is studied by Bejan [25, 26].

If the weight of an heat exchanger is cause for concern in applications such as airborne equipments, the appropriate index for performance scaling may be taken as $I_2 = I_1/\rho$. Here, the best performance is achieved by a foam with $\rho \to 0$ having the largest cell size a (Fig. 8(b)).

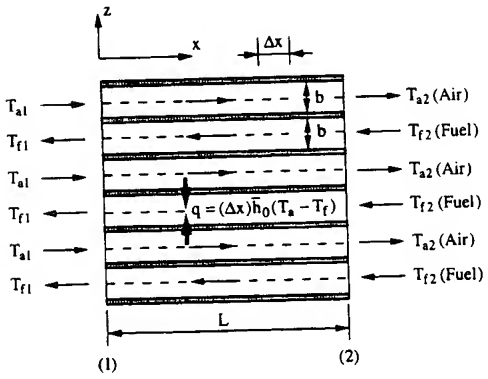

Fig. 11. Prototypical design of a multi-layered counter-current heat exchanger.

6. APPLICATIONS

The model presented in previous sections can be used to analyze a variety of heat exchanger applications where the large surface density of open-celled metal foams is required. Two heat exchanger designs are studied below, one being targeted as the heat sink for next generation multi-chip modules and the other as the air-fuel exchanging system on civil/military aircrafts.

6.1. Heat sinks for power electronic devices

Heat dissipation in high power electronics poses serious challenges for the integration of materials selection with thermal design, circuit design and manufacturing technology [6, 27, 28]. The objective is to select materials that enable the Si chip to operate with high power density (up to 10^7 W/m^2), while maintaining its temperature below that needed to ensure acceptable reliability: usually 90°C.

As an illustration, consider the prototypical design of a compact multi-chip module (MCM) envisioned in Fig. 9. The chips are placed on two plates located at z = 0 and z = b that sandwich an open-

celled foam, with cooling achieved by forced convection through the foam. Both plates are taken to be good dielectrics and conduct heat well such that they are essentially at the same temperature as that of the chips, T_c. The module is thermally insulated at the top and bottom by protective covers (not shown in Fig. 9) and, in addition, no heat is lost in the y-direction. A similar design of package has been analyzed by Lu *et al.* [6] wherein the foam is replaced by a continuum substrate and cooling is achieved around the edges $x = 0$ and $x = L$. It is found that, compared to other package designs considered in Lu *et al.* [7], this particular design suffers from inferior heat dissipation, even when high thermal conductivity substrates with high heat transfer strategies, such as water cooling, are used. However, as elucidated below, the compact design of MCM seems more likely to be successful if a foam with good heat removing capability is used as the substrate, coupled with air or water cooling.

With $\bar{a}$ denoting the distance between the centers of two neighboring chips (Fig. 9), the amount of heat dissipation *per chip* in a module of length $L = l$ is

$$Q_c = 2\lambda_s \mathrm{Bi}^{1/2}\rho^{1/2}\Delta T\left(\frac{\bar{a}^2}{a}\right)\tanh\left(\frac{2\mathrm{Bi}^{1/2}b}{d}\right) \quad (6.1)$$

where $\Delta T = T_c - T_0$. For both water and air cooling, Q_c as a function of ρ is plotted on Fig. 10 for $\lambda_s = 200$ W/(m K), $a = 1$ mm (20 ppi), $\bar{a} = 2$ cm, $\Delta T = 70$°C, and $b/d = 100$. It is seen that, even with forced air convection in a foam with relative density of 0.2, heat is efficiently dissipated from the multi-chip module ($Q_c = 70$ W if air cooling and 490 W if water cooling), indeed making it a very attractive design for micro-electronic devices due to its compactness.

The selection of a substrate material for holding the chips is constrained by many other factors: its thermal expansion must be compatible with the Si chip to minimize the thermally induced stresses, its dielectric constant must be small, should be light weight, and it must not contain any toxic ingredient. The materials that satisfy these requirements include aluminum nitride (AlN), beryllium, aluminum reinforced with particulate silicon carbide and beryllium/silicon carbide composites [6, 29]. Foams made of AlN, for instance, are excellent heat conductors with λ_s up to 300 W/(m K). Since the thermal expansion coefficient of AlN nearly equal that of Si, the residual stresses induced in the chips due to thermal mismatch are very small. The dielectric constant of an AlN foam is exceptionally low if cooling is achieved by forced air,

$$\varepsilon = \varepsilon_f + (\varepsilon_s - \varepsilon_f)\rho \quad (6.2)$$

where $\varepsilon_s = 8.5$ is the dielectric constant of solid AlN and $\varepsilon_f = 1$ the dielectric constant for dry air. All these reasons suggest that AlN and its foams make excellent substrate material for the next-generation chips: indeed, AlN is currently being used by Rockwell International to develop novel high temperature, wide bandgap solid state power devices [30]. Finally, but not least importantly, the cooling strategy of Fig. 9 dictates that "heat spreading" in the substrate emphasized in Lu *et al.* [7] is unnecessary, enabling *high* chip-level power densities at *large* chip densities with $\bar{a} \approx$ chip size.

6.2. Multi-layer heat exchangers

Whilst heat exchangers consisting of a single channel with constant wall temperatures such as that shown in Fig. 1(a) are common, practically it is much more common to design heat exchangers with more complicated geometries to suit the need of transferring heat from one streaming fluid to another. Figure 11 presents the design of a multi-layer counter-current heat exchanger for aeronautical applications where hot air flowing in one direction is used to preheat jet fuel flowing in the opposite direction: this particular design is at present being developed at United Technologies [31]. (It is well-known that a co-current exchanger is less attractive since it always requires a greater length than the counter-current one to perform the same duty.) Each layer consists of an open-celled foam core, thickness b and length L, sandwiched between two thin sheets: the foam and the sheets are made of the same material, usually a high conducting metal such as aluminum or nickel. The layer is infinitely wide in the y-direction with negligible end effects on heat transfer. For air let $\dot{m}_a$, ρ_a, ν_a, T_a and v_a denote its mass flow rate per unit width, density, kinematic viscosity, temperature, and mean velocity inside each layer, respectively. The subscript f will be used to denote the corresponding quantities for the fuel. Subscripts 1 and 2 will refer to the sections corresponding to inlet and outlet of the air layers (or, equivalently, outlet and inlet of the fuel layers). The heat exchanger consists of N identical layers (only six layers are shown in Fig. 11), with hot air flowing in half of them and jet fuel streaming in the rest. The midplane of each layer (dashed line on Fig. 11) is thermally insulated due to symmetry. Denote by $\bar{h}_0$ the overall heat transfer coefficient across each sheet.

The sheet temperature is neither known nor constant for the case considered in Fig. 11, yet one can proceed without knowing it, as demonstrated below. The air-side heat transfer coefficient, $\bar{h}_a$, can still be calculated according to equation (5.21)

$$\bar{h}_a = (\alpha_A/2)\sqrt{h_a\lambda_s d} \quad (6.3)$$

where $\mathrm{Bi}^{1/2}b/d > 2$ has been assumed. This relation also holds for the fuel-side heat transfer coefficient, $\bar{h}_f$, except that the local heat transfer coefficient h_a for air across a bank of cylinders is replaced by h_f for fuel (cf. equation (4.2)). In many situations, the

fluid-related properties, $\bar{h}_a$, $\bar{h}_f$, h_a and h_f, can be safely taken as independent of either temperature or position along the sheet. If the sheets that separate air and fuel are thin and the fouling factor (due either to corrosion products or accumulation of various deposits) is neglected, the overall heat transfer coefficient of the system is given by

$$\frac{1}{\bar{h}_0} = \frac{1}{\bar{h}_a} + \frac{1}{\bar{h}_f} \tag{6.4}$$

If however the sheets are thick or the fouling factor is large, extra terms must be added to equation (6.4) to allow for the additional thermal resistance. Following the method outlined in Section 4.2, an enthalpy balance on the element of the exchanger shown in Fig. 11 gives the total heat transfer rate per unit width, Q, as

$$Q = (NL)\bar{h}_0 \Delta T_m \tag{6.5a}$$

where ΔT_m is the logarithmic mean temperature difference defined by

$$\Delta T_m = \frac{(T_{a2} - T_{f2}) - (T_{a1} - T_{f1})}{\ln[(T_{a2} - T_{f2})/(T_{a1} - T_{f1})]} \tag{6.5b}$$

If the velocity of air is high at a high temperature, then $T_{a1} \approx T_{a2}$ and $\bar{h}_0 \approx \bar{h}_f$, in which case equations (6.5a)–(b) reduce to that corresponding to a single duct system having a constant wall temperature.

The pressure drop in the air layer Δp_a follows directly from equation (5.26) as

$$\Delta p_a = (2L/a) f_a \chi_a \rho_a v_{a\,max}^2 \tag{6.6}$$

where the maximum velocity in the layer is given by

$$v_{a\,max} = \frac{2\dot{m}_a}{Nb\rho_a(1 - d/a)} \tag{6.7}$$

On the fuel side, the pressure drop is calculated from equations (6.6) and (6.7) with each subscript a replaced by f. Since the pressure drop varies at $LN^{-m}b^{-m}$ with $m \approx 1.84$, we can always select the best combination of L, N and b to lower the pumping power once it becomes unacceptable. A high pressure drop not only increases the operational cost but often also leads to intolerable noises. One of the advantages of designing exchangers with foams is that they still offer excellent heat transfer coefficient even if the mean flow velocity falls below the critical value required to maintain turbulent flow in an otherwise foam-free duct. Thus, whilst the layer thickness b is limited by the foam cell size a, the restriction placed on the total number of layers is much less stringent. Also, the foam itself may act as a noise suppressor due to its sound absorption capabilities.

Acknowledgements—This work was supported by EPSRC (No. EJA S67) and by the ARPA/ONR MURI program (No. N00014-1-96-1028). T. J. L. wishes to thank A. G. Evans, A. Bastawros and D. Zhang (Harvard University), B. Leyda (ERG) and L. J. Gibson (MIT) for many insightful discussions.

REFERENCES

1. Gibson, L. J. and Ashby, M. F., *Cellular Solids*, 2nd Edn. Cambridge University Press, Cambridge, 1997.
2. Tien, C. L. and Vafai, K., *Adv. Appl. Mech.*, 1990, **27**, 225.
3. Collishaw, P. G. and Evans, J. R. G., *J. Mater. Sci.*, 1994, **29**, 486.
4. Leyda, B., private communication, 1997.
5. Beavers, G. S. and Sparrow, E. M., *J. Appl. Mech.*, 1969, **36**, 711.
6. Lu, T. J., Evans, A. G. and Hutchinson, J. W., *Trans. ASME J. Electronic Packaging*, 1998, **120**.
7. Antohe, B. V., Lage, J. L., Price, D. C. and Weber, R. M., *Int. J. Heat Fluid Flow*, 1996, **17**, 594.
8. Kaviany, M., *Int. J. Heat Mass Transfer*, 1985, **28**, 851.
9. Bejan, A., *Heat Transfer*. John Wiley & Sons, 1993.
10. Koh, J. C. Y. and Colony, R., *J. Heat Transfer*, 1974, **96**, 324.
11. Vafai, K. and Tien, C. L., *Int. J. Heat Mass Transfer*, 1981, **24**, 195.
12. Bastawros, A.-F. and Evans, A. G., *Proceedings of the Symposium on the Application of Heat Transfer in Microelectronics Packaging*. IMECE, Dallas, TX, 1997.
13. Carslaw, H. S. and Jaeger, J. C., *Conduction of Heat in Solids*. Oxford University Press, 1959.
14. Gosse, J., *Technical Guide to Thermal Processes*. Cambridge University Press, 1981.
15. Kay, J. M. and Nedderman, R. M., *Fluid Mechanics and Transfer Processes*. Cambridge University Press, 1985.
16. Holman, J. P., *Heat Transfer*. McGraw-Hill Book Company, New York, 1989.
17. Becker, M., *Heat Transfer—A Modern Approach*. Plenum Press, 1986.
18. Grimson, E. D., *Trans. ASME*, 1937, **59**, 583–594.
19. Kreith, F. and Black, W. Z., *Basic Heat Transfer*. Harper & Row, New York, 1980.
20. Zukauskas, A. A., *Handbook of Single-Phase Convective Heat Transfer*, ed. S. Kakac *et al.* Wiley, New York, 1987.
21. Shah, R. K., *Heat Exchangers: Thermal-Hydraulic Fundamentals and Design*, ed. S. Kakac, A. E. Bergles and F. Mayinger. Hemisphere, Washington, DC, 1981.
22. Bejan, A., *Convective Heat Transfer*. Wiley, New York, 1984.
23. Jakob, M., *Trans. ASME*, 1938, **60**, 384.
24. Schlegel, A., Benz, P. and Buser, S., *Wärme und Stoffübertragung*, 1993, **28**, 259.
25. Bejan, A., *Int. J. Heat Mass Transfer*, 1992, **35**, 3259.
26. Bejan, A., *J. Heat Transfer*, 1995, **117**, 767.
27. Blodgett, A. J. and Barbour, D. R., *IBM J. Res. Develop.*, 1982, **26**, 30.
28. Bar-Cohen, A. and Kraus, A. D. (ed.), *Advances in Thermal Modelling of Electronic Components and Systems*, Vol. I. Hemisphere, New York, 1988.
29. Ashby, M. F. and Cebon, D., *Cambridge Materials Selector: Case Studies in Materials Selection*. Granta Design Limited, Cambridge, U.K., 1996.
30. Shaw, M. C., private communication, 1997.
31. Evans, A. G., private communication, 1997.
32. Jain, S. C. and Krishnan, K. S., *Proc. R. Soc. London A*, 1954, **222**, 167.

APPENDIX A

Heat transfer due to radiation and convection from a heated cylinder

Consider a thin, isolated cylinder of uniform temperature T and diameter d, standing in a transverse flow of uniform temperature $T_f (< T)$. The amount of heat transfer due to convection per unit length of the cylinder is

$$q_h = (\pi d)h(T - T_f) \tag{A.1}$$

while that due to radiation per unit length is approximately

$$q_r = (\pi d)h_r(T - T_f) \tag{A.2}$$

Here, h is the average convective heat transfer coefficient and h_r the effective radiative heat transfer coefficient given by

$$h_r = \sigma\varepsilon(T^2 + T_f^2)(T + T_f) \tag{A.3}$$

where $\sigma = 5.67 \times 10^{-8}$ W/(m^2 K^4) is the Stefan–Bolzmann constant and ε is the normal total emissivity of the surface. For aluminum, ε is in the range 0.04–0.2 [16], and the maximum service temperature for aluminum-based metal foams is about 500 K [2]. For turbulent flows which are expected to occur in a bank of cylinders representative of metal foams, the convective heat transfer coefficient h calculated from equation (4.2) is typically on the order of $10^2 \sim 10^4$ W/(m^2 K), while that of the radiative coefficient h_r based on equation (A.3) is $10^0 \sim 10^1$ W/(m^2 K). Consequently, heat transfer due to radiation is negligible if metal foams are applied in heat exchangers involving turbulent flow of fluid. At temperatures above 1000 K, radiation is expected to play an important role in electrically heated thin wires made of refractory metals [32].